Supporting Information

Mixed Valence of Bismuth in Hexagonal Chalcohalide Nanocrystals

Danila Quarta,[a†] Stefano Toso,[b,c†] Gabriele Saleh,[b] Rocco Caliandro,[d]* Anna Moliterni,[d] Andrea Griesi,[b] Giorgio Divitini,[b] Ivan Infante,[b,e,f] Giuseppe Gigli,[a,g] Cinzia Giannini,[d] Liberato Manna,[b] Carlo Giansante[a]**

[a] *Consiglio Nazionale delle Ricerche, Istituto di Nanotecnologia − CNR NANOTEC, Via Monteroni, 73100 Lecce − Italy*

[b] *Istituto Italiano di Tecnologia − IIT, Via Morego 30, 16163 Genova − Italy*

[c] *International Doctoral Program in Science, Università Cattolica del Sacro Cuore, 25121 Brescia – Italy*

[d] *Consiglio Nazionale delle Ricerche, Istituto di Cristallografia − CNR IC, Via Amendola 122, 70126 Bari – Italy*

[e] *BCMaterials, Basque Center for Materials, Applications, and Nanostructures, UPV/EHU Science Park, Leioa 48940 – Spain*

[f] *Ikerbasque, Basque Foundation for Science, Bilbao 48009 – Spain*

[b] *Dipartimento di Fisica, Unisalento, Via per Arnesano, 73100 Lecce − Italy*

[†] These authors contributed equally

* e-mails: gabrielesaleh@outlook.com; rocco.caliandro@ic.cnr.it; carlo.giansante@nanotec.cnr.it

Synthetic Parameters.

Table S1. Standard synthetic conditions chosen to prepare the colloidal NCs of hexagonal Bi chalcohalide.

Synthetic Product	Injection/Growth Temperature (°C)	Growth Time (min)	Bi precursor concentration (mM)	Oleic acid concentration (M)	E precursor concentration (mM)	X precursor concentration (mM)
$Bi_{13}S_{18}Br_2$	180	15	63	0.63	32	32
$Bi_{13}S_{18}I_2$	180	15	63	0.63	32	11

Table S2. Range of the synthetic conditions yielding phase pure colloidal NCs of hexagonal Bi chalcohalide, which were used to attempt a control of their size and shape.

Synthetic Product	Injection/Growth Temperature (°C)	Growth Time (min)	Bi acetate concentration (mM)	Oleic acid concentration (M)	Bi:E molar ratio	Bi:X molar ratio
$Bi_{13}S_{18}Br_2$	180	1 – 180	63	0.63 – 6.3	2, $(TMS)_2S$	2, BzBr
	180	15	63	0.63	2, $(TMS)_2S$	2, TMSBr
	180	60	63	0.63	2, thiourea	2, BzBr
$Bi_{13}S_{18}I_2$	180	15	63	0.63	2, $(TMS)_2S$	6, BzI
	180	15	63	0.63	2, $(TMS)_2S$	6, TMSI

Structural Refinement Parameters.

Table S3. Refinement parameters derived from the PDF fits. R_w is the weighted agreement factor between observed and calculated PDF, Delta1 is the coefficient for $1/r$ contribution to the peak sharpening, Q_{broad} describes the peak broadening from increased intensity noise at high Q, $SP_{diameter}$ is the particle diameter for PDF shape damping function, E_{rad} and P_{rad} are respectively the equatorial and polar radii for the ellipsoidal shape damping function.

	$Bi_{12.67}S_{18}Br_2$	**$Bi_{13}S_{18}Br_2$** (joint refinement of two separated dimers)
R_w	0.078	0.083
Delta1	0.30	1.54
Q_{broad}	0.011	
$SP_{diameter}$ (Å)	68.8	
E_{rad}, P_{rad} (Å)		33.3, 33.3
a,b,c (Å)	15.514, 15.514, 4.022	15.463, 15.463, 8.022

Table S4. Figures of merit obtained by the XPD refinement. Agreement factors provided by Fullprof at the end of the Rietveld refinement. R_p is the agreement factor between observed and calculated profile, R_{wp} is the weighted- profile reliability parameter, χ^2 is the chi-squared distribution, GoF is the Goodness of Fit.

	$Bi_{12.67}S_{18}Br_2$	**$Bi_{13}S_{18}Br_2$**
R_p (%)	4.22	4.24
R_{wp} (%)	5.74	5.87
χ^2	2.43	2.58
GoF	1.5	1.6

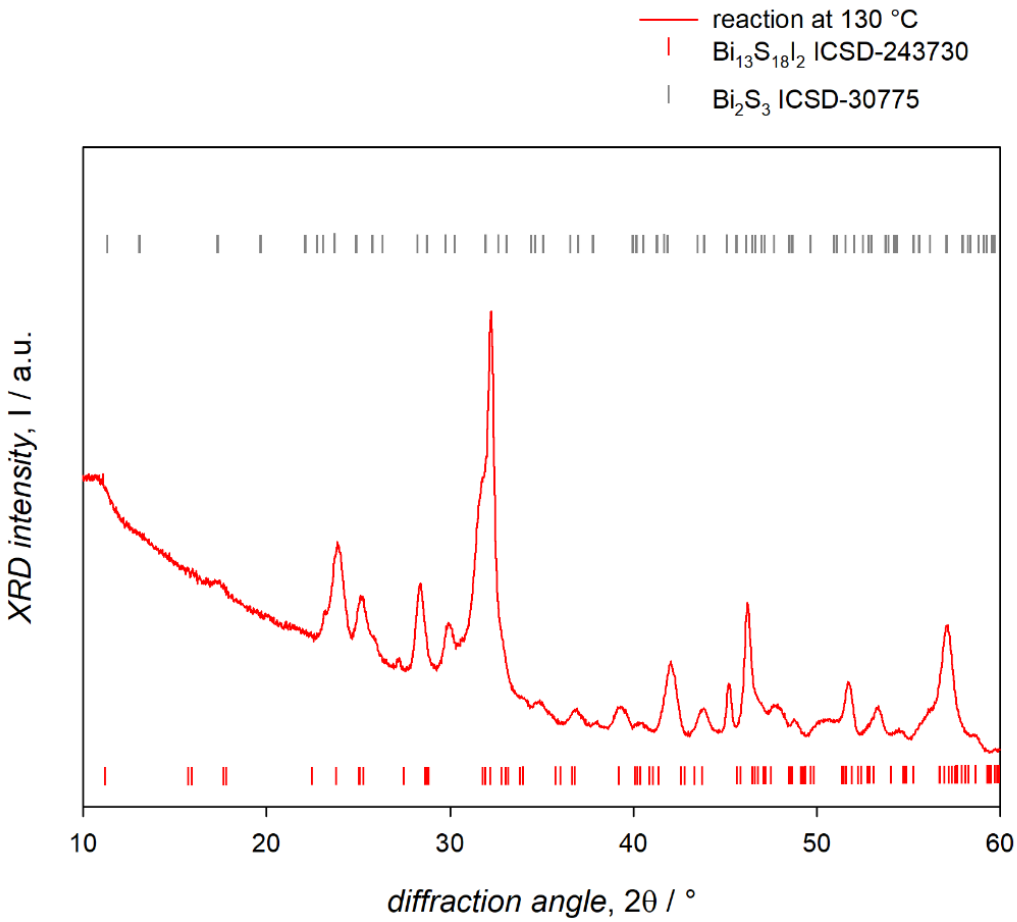

Figure S1. XPD pattern of the synthetic product obtained with a reaction temperature of 130 °C.

Colloidal $Bi_{13}S_{18}Br_2$ NCs.

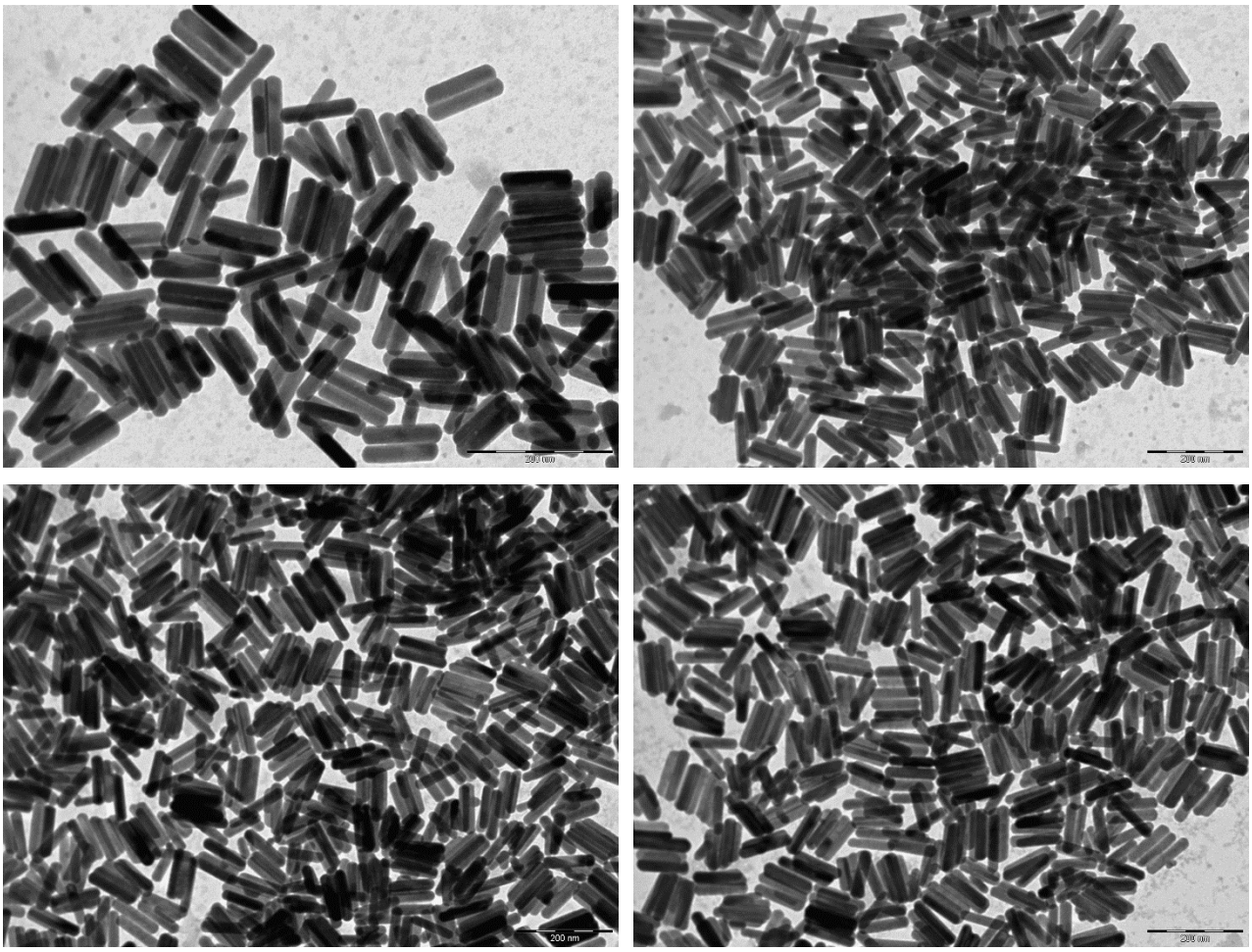

Figure S2. TEM images of the colloidal NCs of Bi sulfobromide prepared by using bis(trimethylsilyl)sulfide and benzoylbromide as S and Br precursors, respectively.

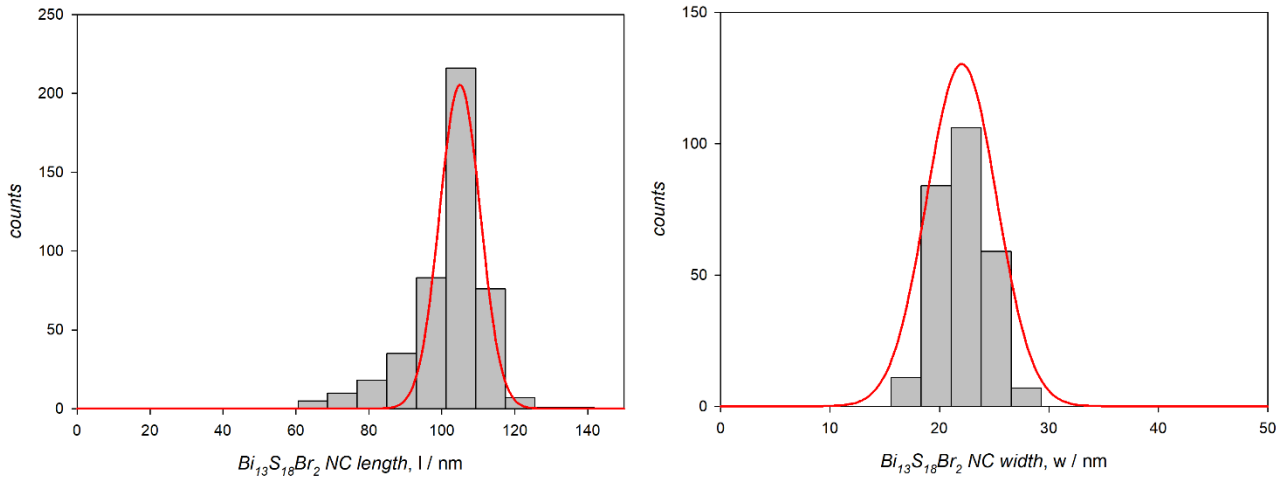

Figure S3. Polydispersity of both the length and the width of the colloidal NCs of Bi sulfobromide.

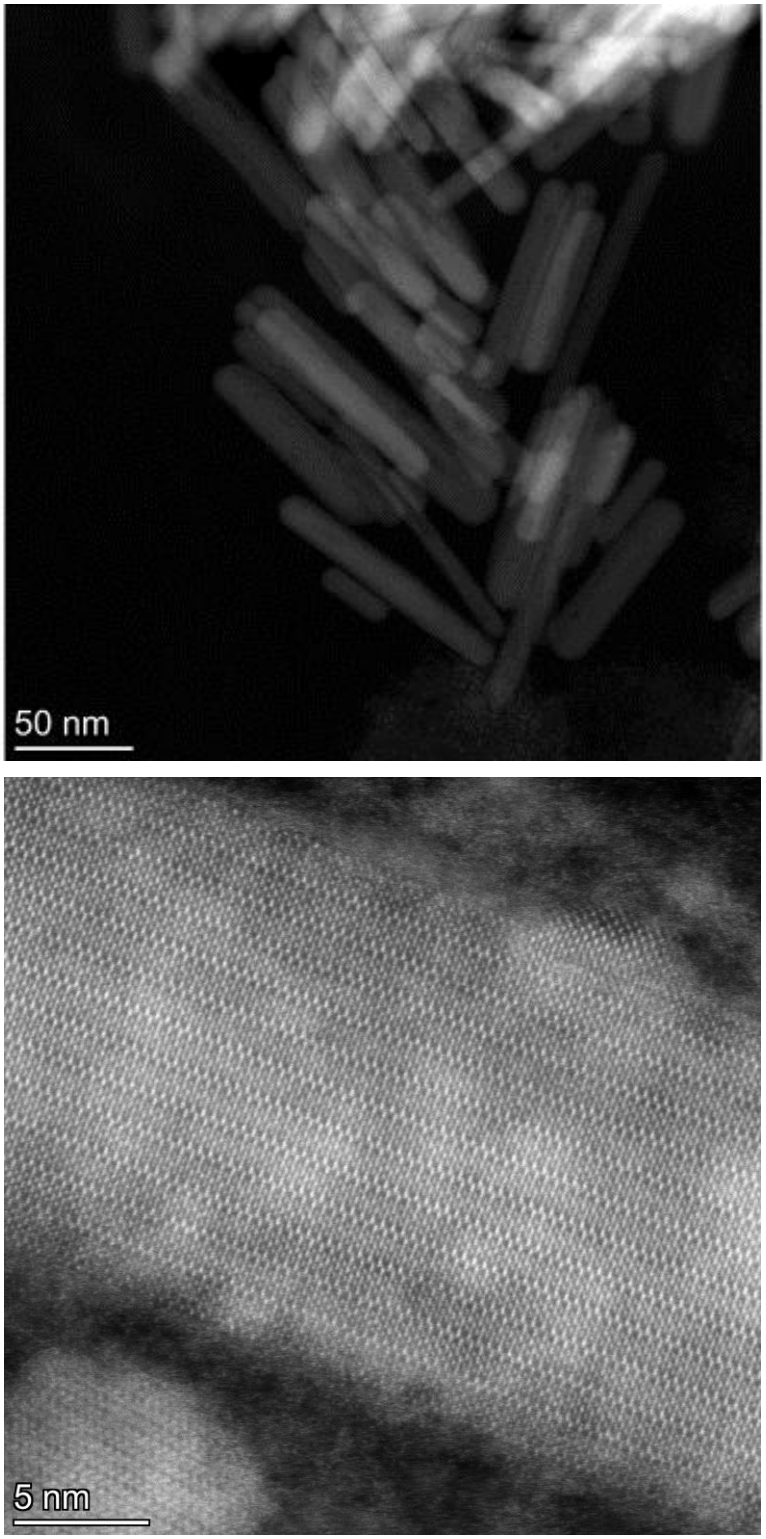

Figure S4. HAADF-STEM images of the colloidal NCs of Bi sulfobromide.

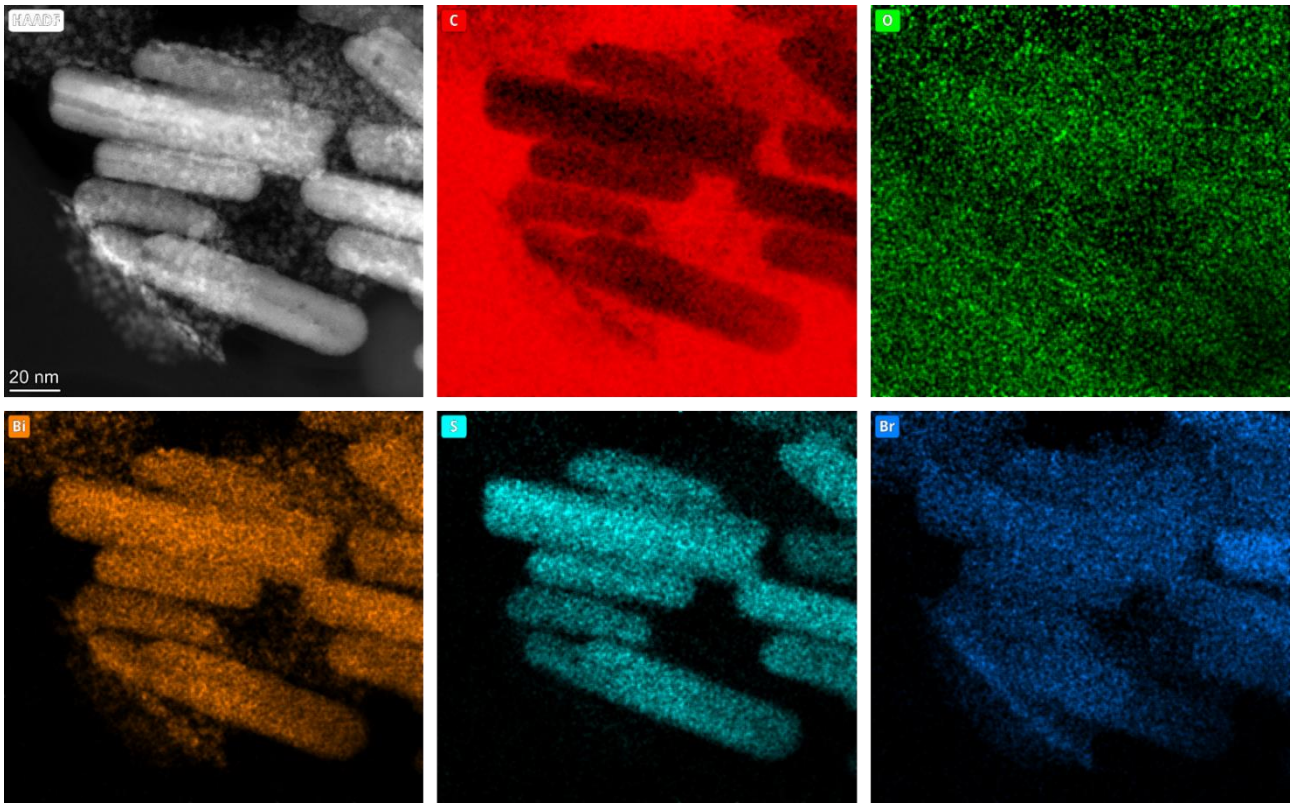

Figure S5. EDX reference high-angle annular dark field image and elemental maps of the colloidal NCs of Bi sulfobromide. The chemical composition is homogeneous.

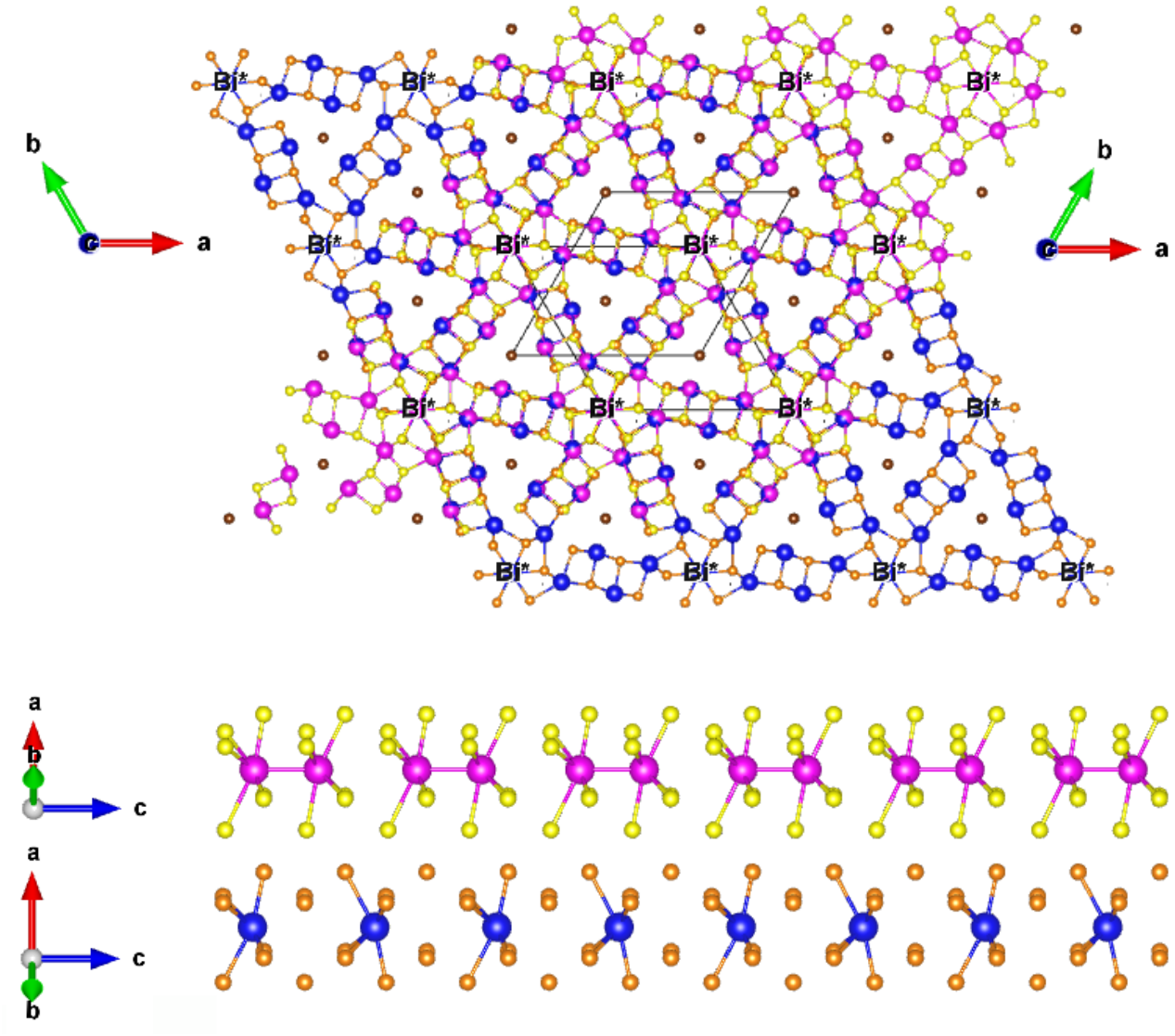

Figure S6. Superimposed models of the $Bi_{13}S_{18}Br_2$ (pink Bi and yellow S) and $Bi_{12.67}S_{18}Br_2$ (blue Bi and orange S) structures and detail on the S coordination of the columnar Bi atoms in these two structures (which are marked as Bi* in the superimposed structure).

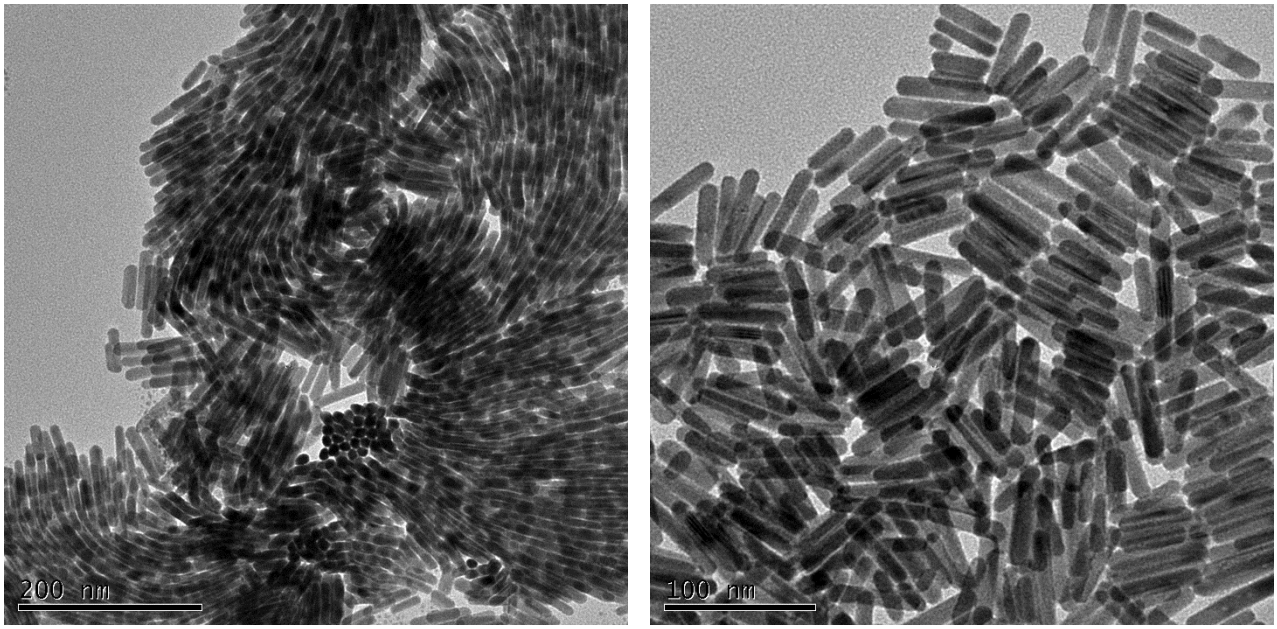

Figure S7. TEM images of the colloidal NCs of Bi sulfobromide prepared by using bis(trimethylsilyl)sulfide and trimethylsilylbromide as S and Br precursors, respectively.

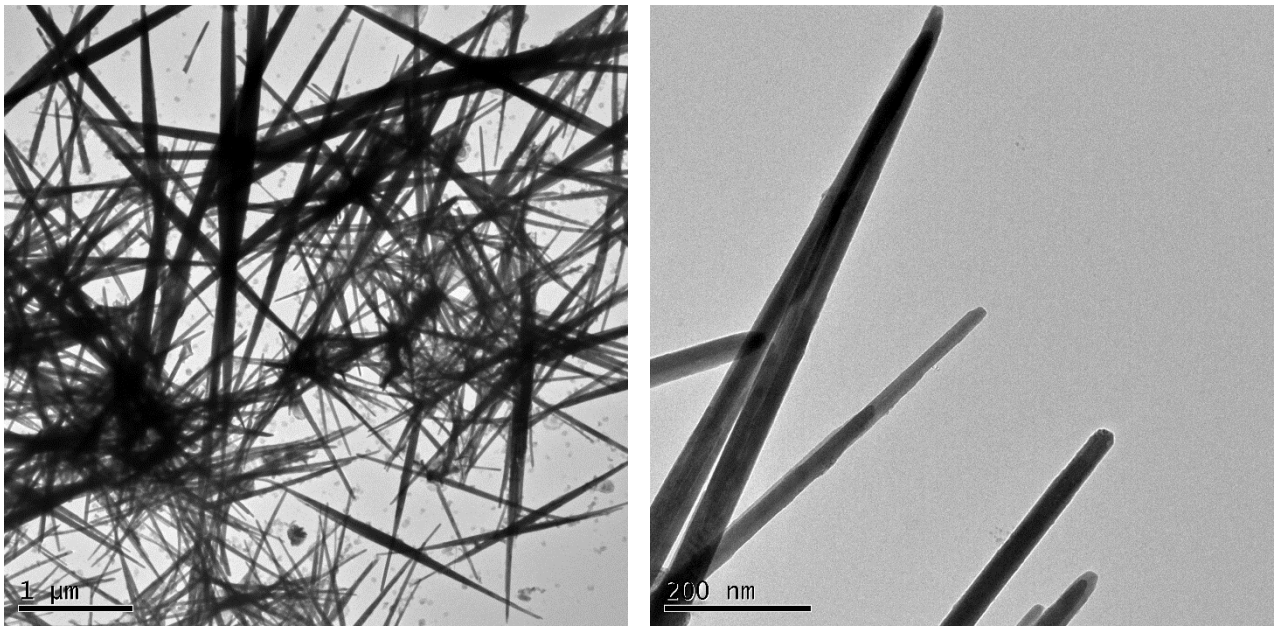

Figure S8. TEM images of the colloidal NCs of Bi sulfobromide prepared by using tetramethylthiourea and benzoylbromide as S and Br precursors, respectively.

Colloidal $Bi_{13}S_{18}I_2$ NCs.

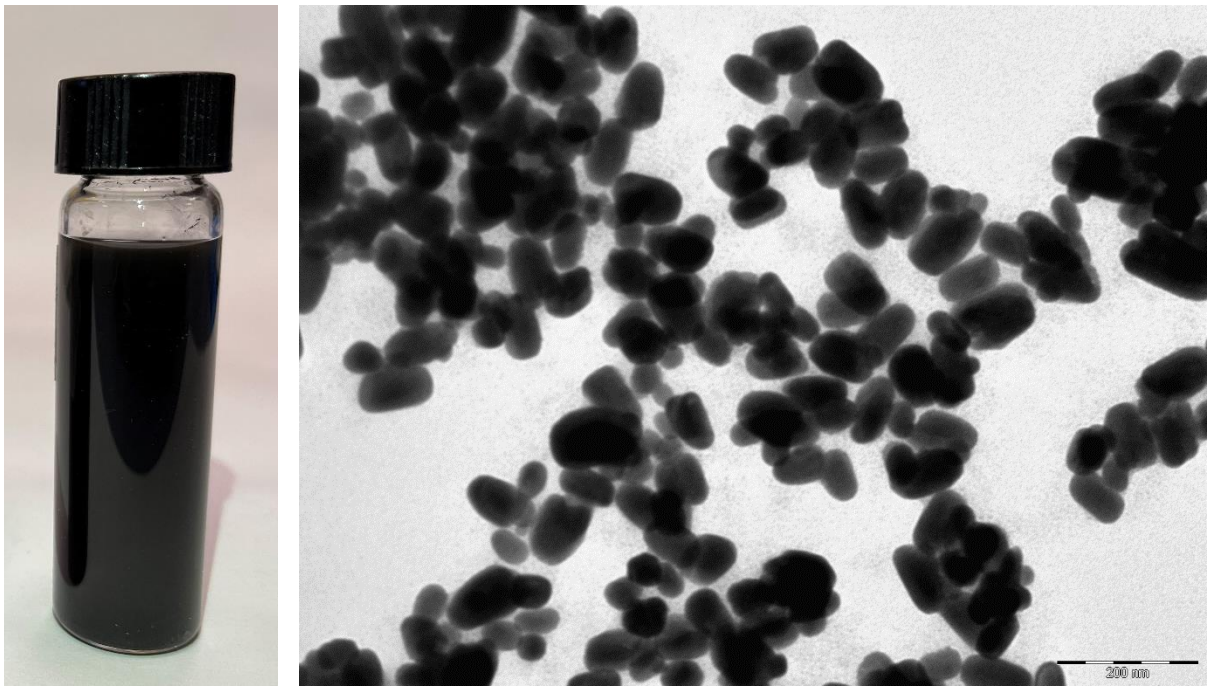

Figure S9. Daylight picture of a toluene dispersion of the colloidal NCs of Bi sulfoiodide and TEM image; the colloidal NCs were prepared by using bis(trimethylsilyl)sulfide and benzoyliodide as S and I precursors, respectively.

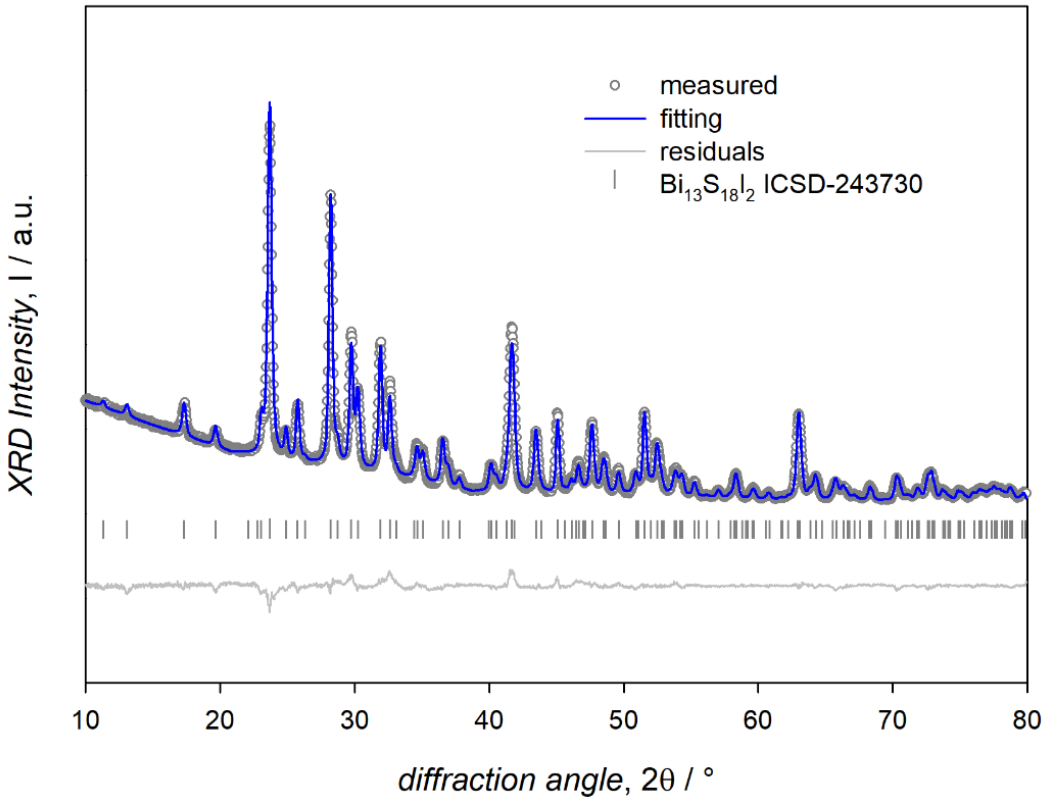

Figure S10. Rietveld refinement of the XRD pattern of the colloidal NCs of Bi sulfoiodide.

Optical Absorption of the hexagonal Bi sulfohalide NCs and their Calculated Electronic Structure.

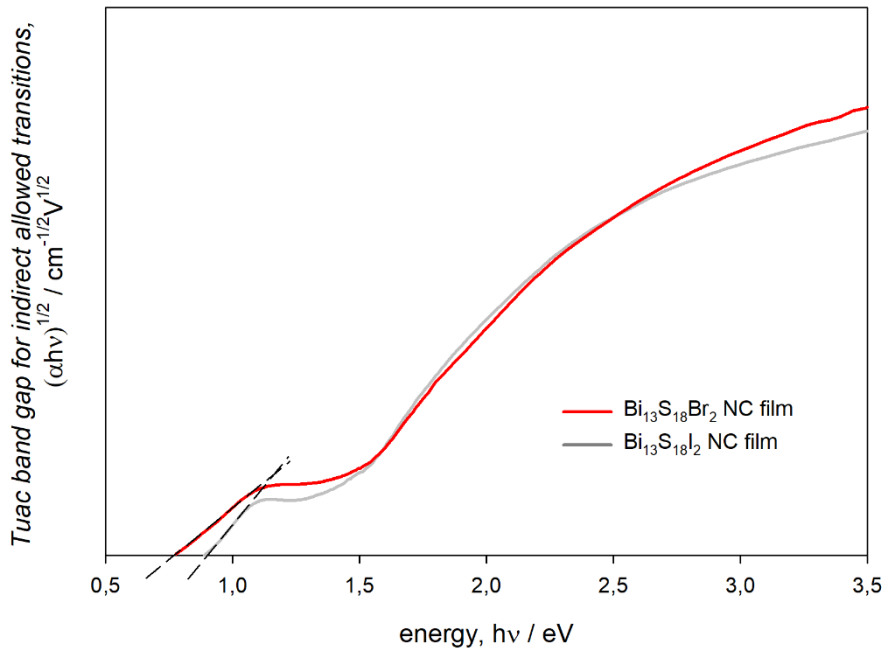

Figure S11. Linear fit of the absorption edge of the NC films according to the Tauc representation for estimating the band gap in the case of indirect, allowed transitions.

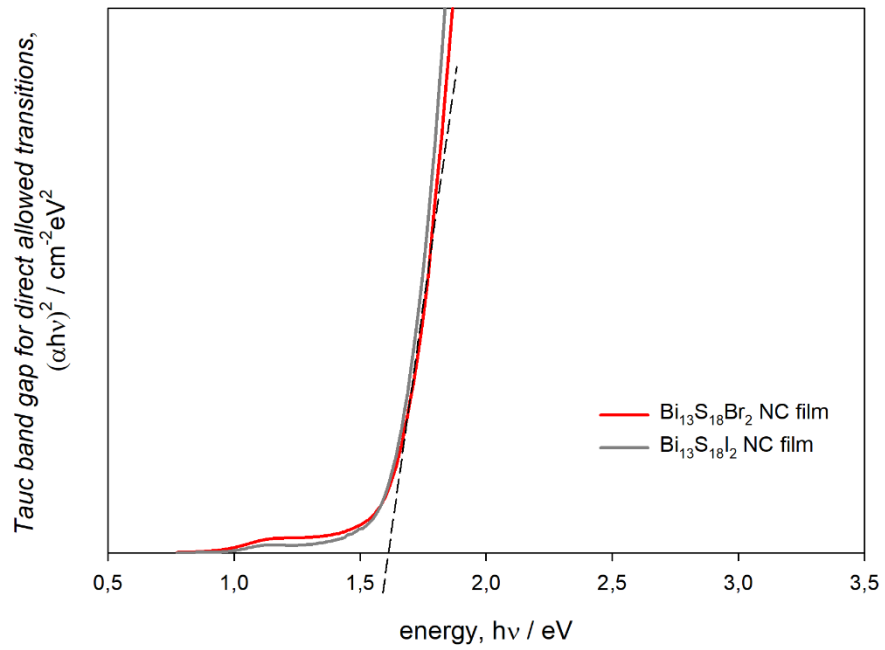

Figure S12. Linear fit of the absorption edge of the NC films according to the Tauc representation for estimating the band gap in the case of direct, allowed transitions.

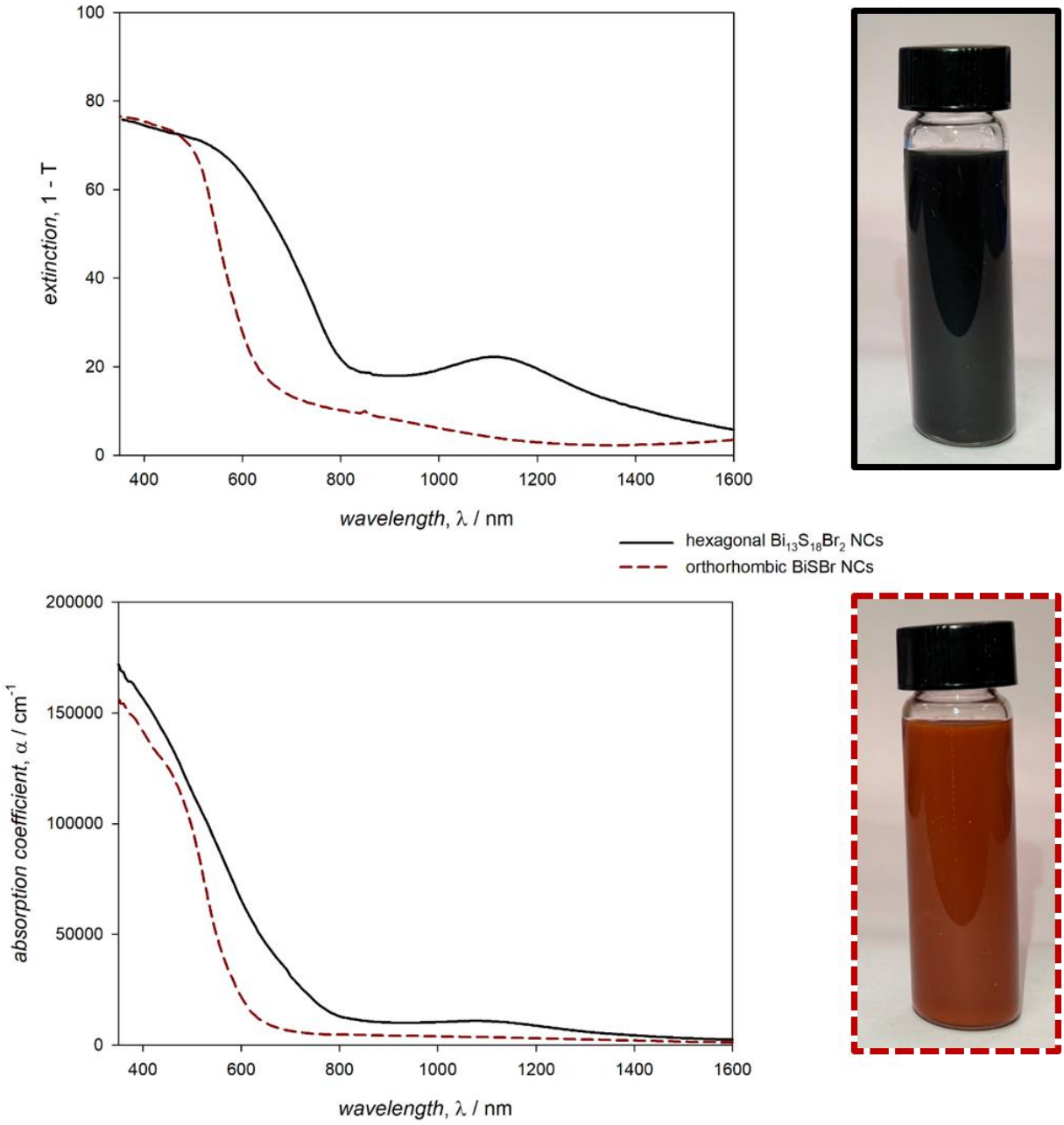

Figure S13. Optical extinction (top) and absorption coefficient (bottom) spectra of NC thin films. Vials of BiSBr and $Bi_{13}S_{18}Br_2$ NC toluene dispersions are shown to highlight color differences.

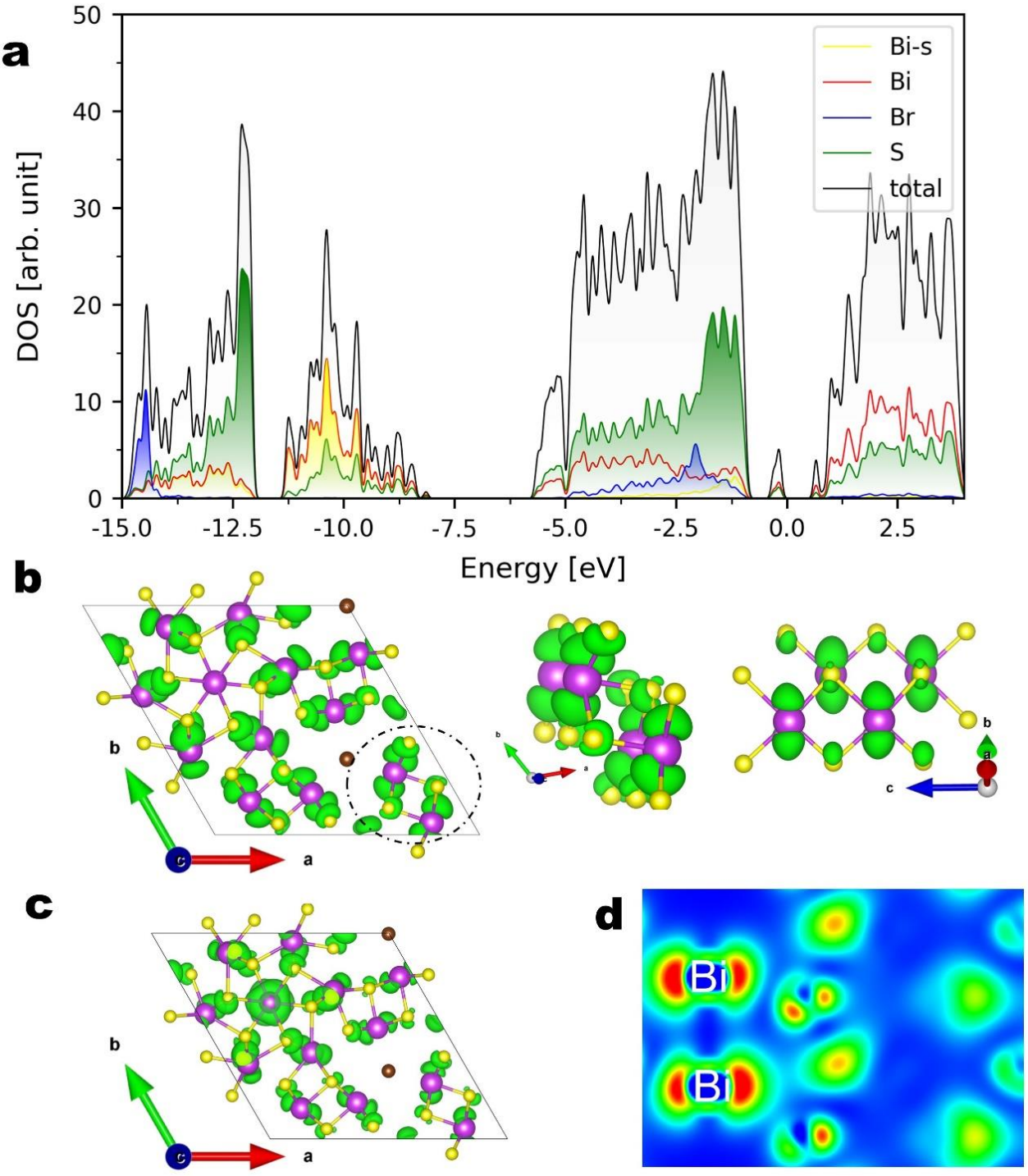

Figure S14. DOS of $Bi_{13}S_{18}Br_2$ (a) and partial charge densities of the conduction band bottom shown as green isosurfaces (b,c) and 2D color map (d). The partial charge density is the charge density evaluated including only those electronic states lying in the following energy ranges (with respect to the Fermi level): +0.5/+0.8 eV (b) and +0.8/1.1 eV (c,d). Note that the partial density in panel b corresponds to the first small DOS peak above the Fermi level seen in panel a. Two enlargements on a Bi/S fragment circled in the picture are also shown. The isovalues (VASP units) in panel b (c) is 0.00025 (0.001). In panel d, a 2D map of the partial charge density of panel c is plotted onto a plane parallel to the b,c crystallographic plane and passing through the Bi atoms forming the dimer. The blue-green-red color scale ranges from 0.0 to 0.002 (VASP units).

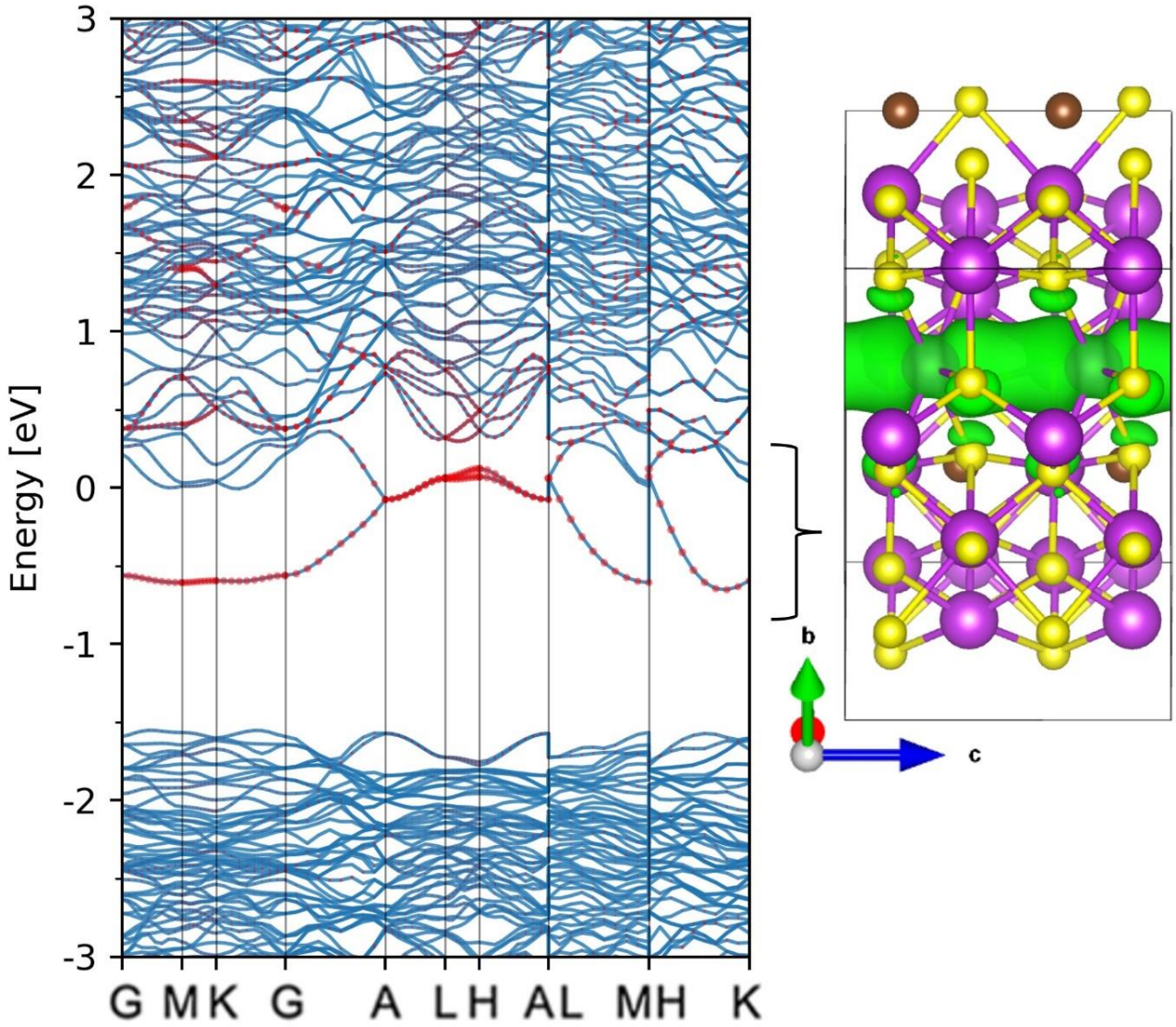

Figure S15. Band structure and partial charge density for the $Bi_{13}S_{18}Br_2$ compound with 'columnar' Bi atoms (see main text for definition) equidistant. Note its metallic character. The projection on Bi atoms forming the dimer is shown as red dots on the band structure. On the right, the partial charge density corresponding to the states around the Fermi level (from -0.75 to +0.15 eV) is shown as green isosurfaces (isovalue: 0.0016 in VASP units).

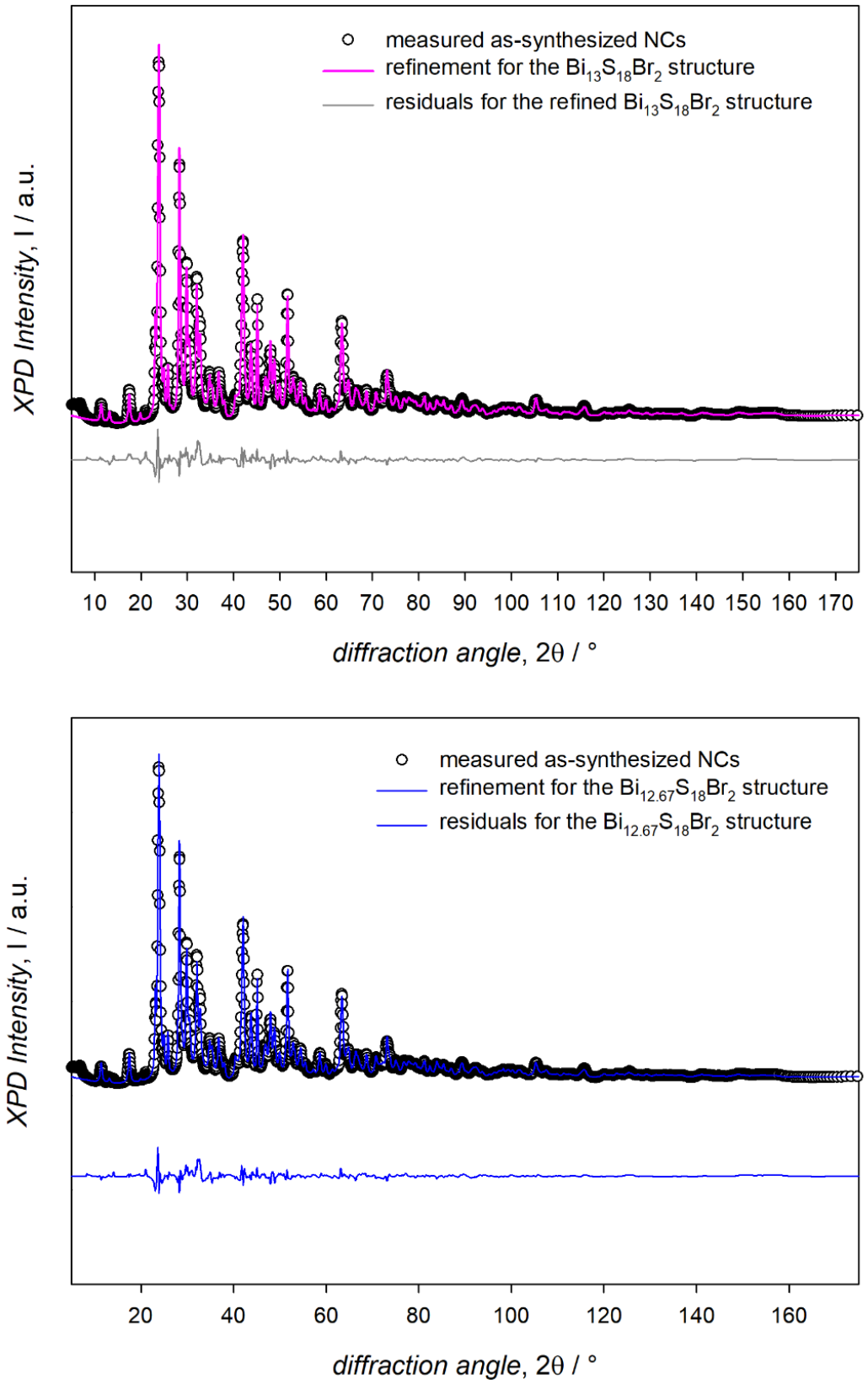

Figure S16. Rietveld refinement of the XPD pattern of the as-synthesized colloidal NCs using either $Bi_{13}S_{18}Br_2$ or $Bi_{12.67}S_{18}Br_2$ models (to facilitate the comparison with data collected on lab-grade setups, the 2θ values of the XPD horizontal axis were converted to emulate the CuKα_1 radiation). The Rietveld refinement of XPD data yielded comparably good fits for both structures.

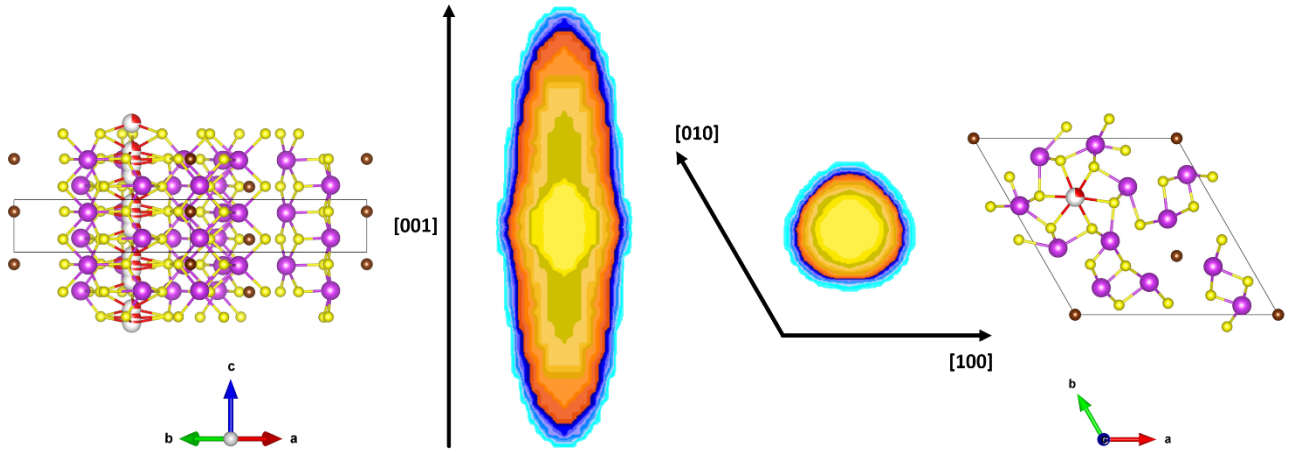

Figure S17. Image of the refined $Bi_{13}S_{18}Br_2$ crystallite spherical harmonics diagram.

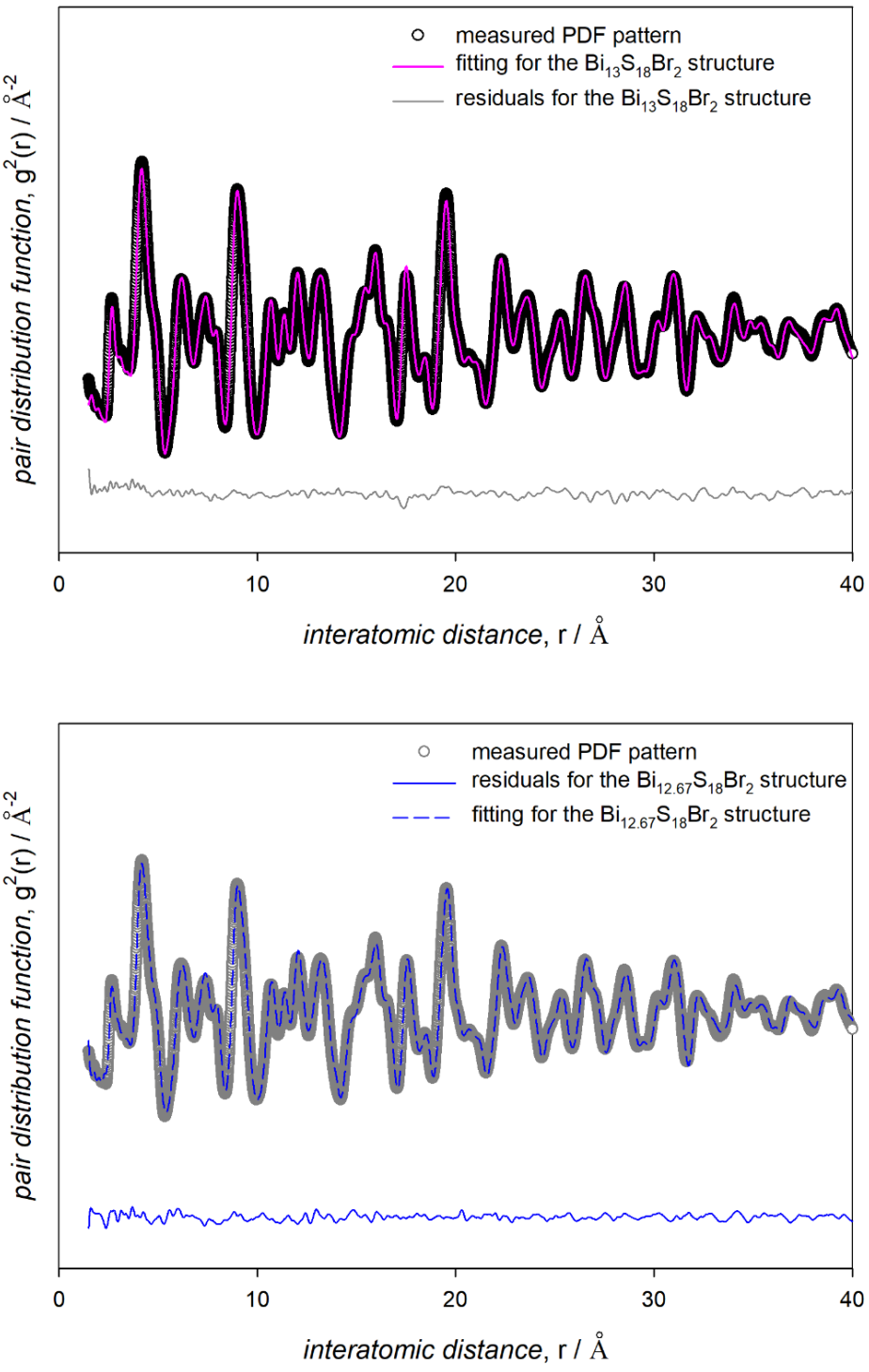

Figure S18. PDF profiles of the as-synthesized NCs using either the $Bi_{13}S_{18}Br_2$ (top) or $Bi_{12.67}S_{18}Br_2$ (bottom) models. The refinement of the PDF data initially gave a worse agreement for $Bi_{13}S_{18}Br_2$ than for $Bi_{12.67}S_{18}Br_2$. However, this was due to an inadequate description of the positional disorder of the Bi_2^{4+} dimers. In fact, while for the Rietveld refinement the disorder can be modelled by including in the structural model multiple dimers with partial occupancy, the inclusion of partially occupied dimers in the PDF refinement result in improper interatomic distances among overlapping dimers. This deadlock was solved by generating four models out of the published $Bi_{13}S_{18}Br_2$ structure, each containing a fully occupied Bi_2^{4+} dimer in a different position, by checking those producing distinct PDF profiles (two), then refining these two models simultaneously against the PDF data. The atomic parameters of the two phases were constrained to be equal, apart for the positions of the Bi^{2+} ions of the dimers, which were refined independently. On this basis, fitting of the PDF data produced comparable results for both the $Bi_{13}S_{18}Br_2$ and the $Bi_{12.67}S_{18}Br_2$ structures.

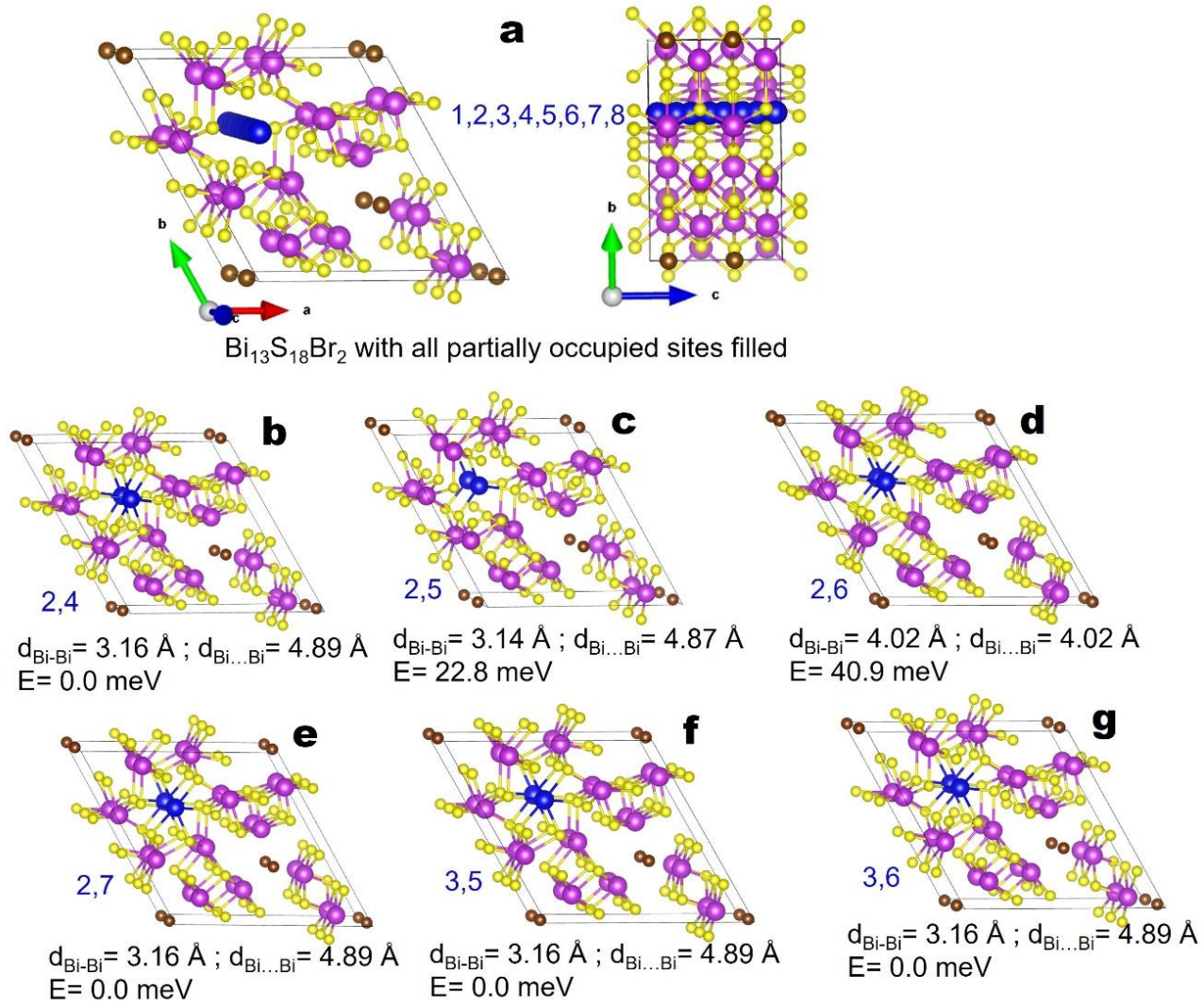

Figure S19. Investigated Bi configurations in $Bi_{13}S_{18}Br_2$. Disordered Bi atoms shown in blue. Panel a reports the structure showing all the 8 partially occupied Bi sites, in two different orientations. The remaining panels report the DFT optimized structures of various configurations (the structures with Bi atoms closer than 2.5 Å were not investigated as expected to have high energy). The blue number report which of the 8 Bi sites are occupied in the initial structure. Below each structure, the two Bi-Bi distances in the DFT optimized structure are reported, along with the energy with respect to the lowest energy configuration. Note that there are several energetically equivalent Bi positions. This indicates that, in the real crystal, two rows of Bi atoms (both extending along the c direction and differing by the position on the a,b crystallographic plane, i.e. lying in different unit cells) can have Bi atoms on different positions along the c axis, thus giving rise to the observed crystallographic disorder. As these calculations were meant to obtain qualitative results, the plane-wave kinetic energy cutoff was set to 400 eV, and the unit cell parameters were fixed at the experimental estimate. The remaining computational settings were as described in the main text.

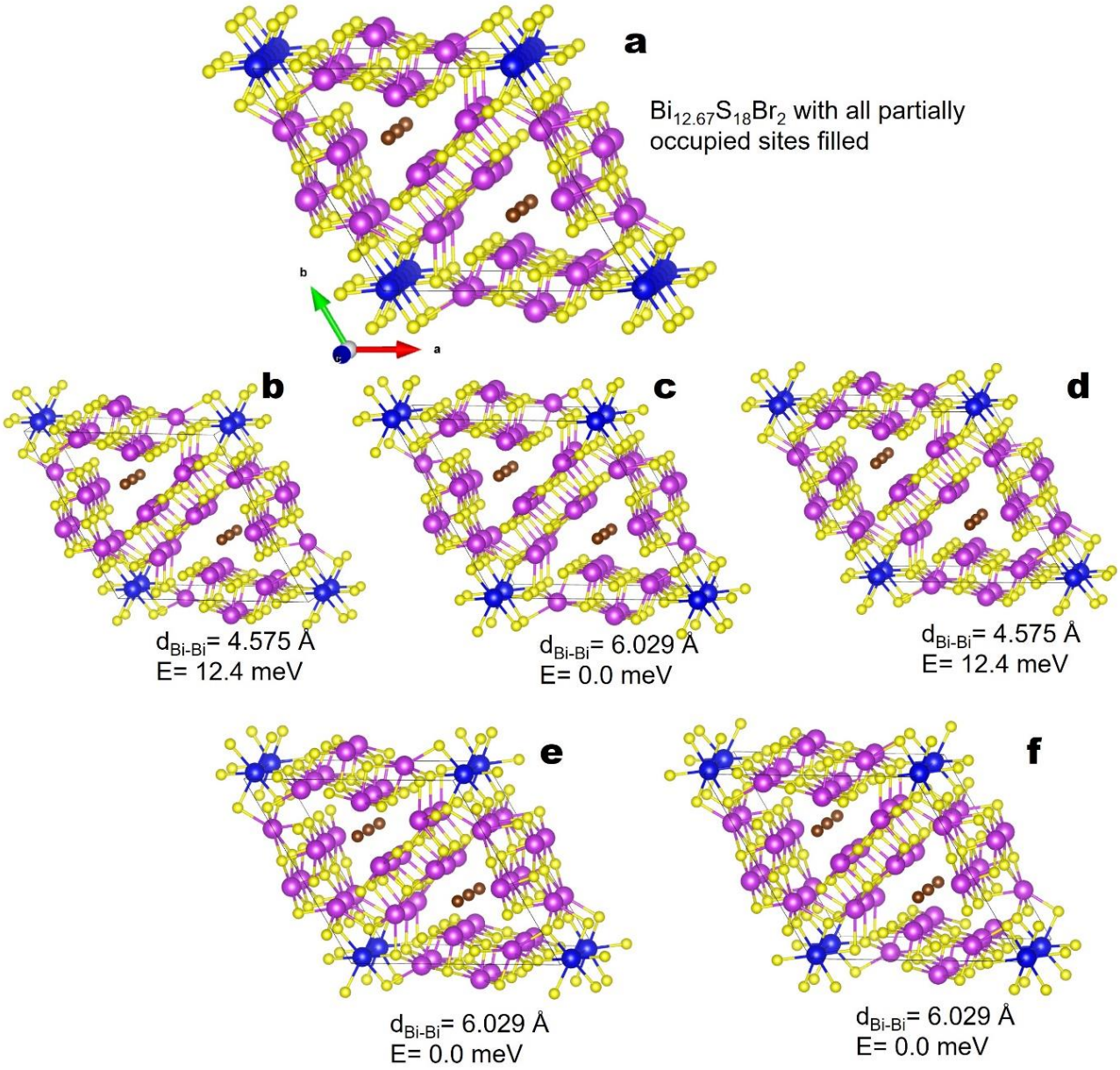

Figure S20. Investigated Bi configurations in $Bi_{12.67}S_{18}Br_2$. Disordered Bi atoms shown in blue. Panel a reports the structure showing all partially occupied Bi sites, while the remaining panels report the DFT optimized structures of various configurations (the structures with Bi atoms closer than 2.5 Å were not investigated as expected to have high energy), their energy with respect to the minimum energy configuration, and the distance between disordered Bi atoms. The final structure in panel d is energetically equivalent to that of panel b, and the structures in panels c,e,f are all minimum energy configurations. In particular, the structures c, e, and f are related by a rigid translation of the two Bi disordered atoms. This indicates that, in the real crystal, two rows of Bi atoms (both extending along the c direction and differing by the position on the a,b crystallographic plane) can have Bi atoms on different positions along the c axis, thus giving rise to the observed crystallographic disorder. Moreover, the relatively low energy of other configurations (lower than the thermal energy at room T), suggests that the disordered Bi atoms may be able to dynamically migrate among the various accessible Bi positions of panel a. As these calculations were meant to obtain qualitative results, the plane-wave kinetic energy cutoff was set to 259 eV (the highest value among those suggested in the adopted pseudopotential), and the unit cell parameters were fixed at the experimental estimate. The remaining computational settings were as described in the main text.

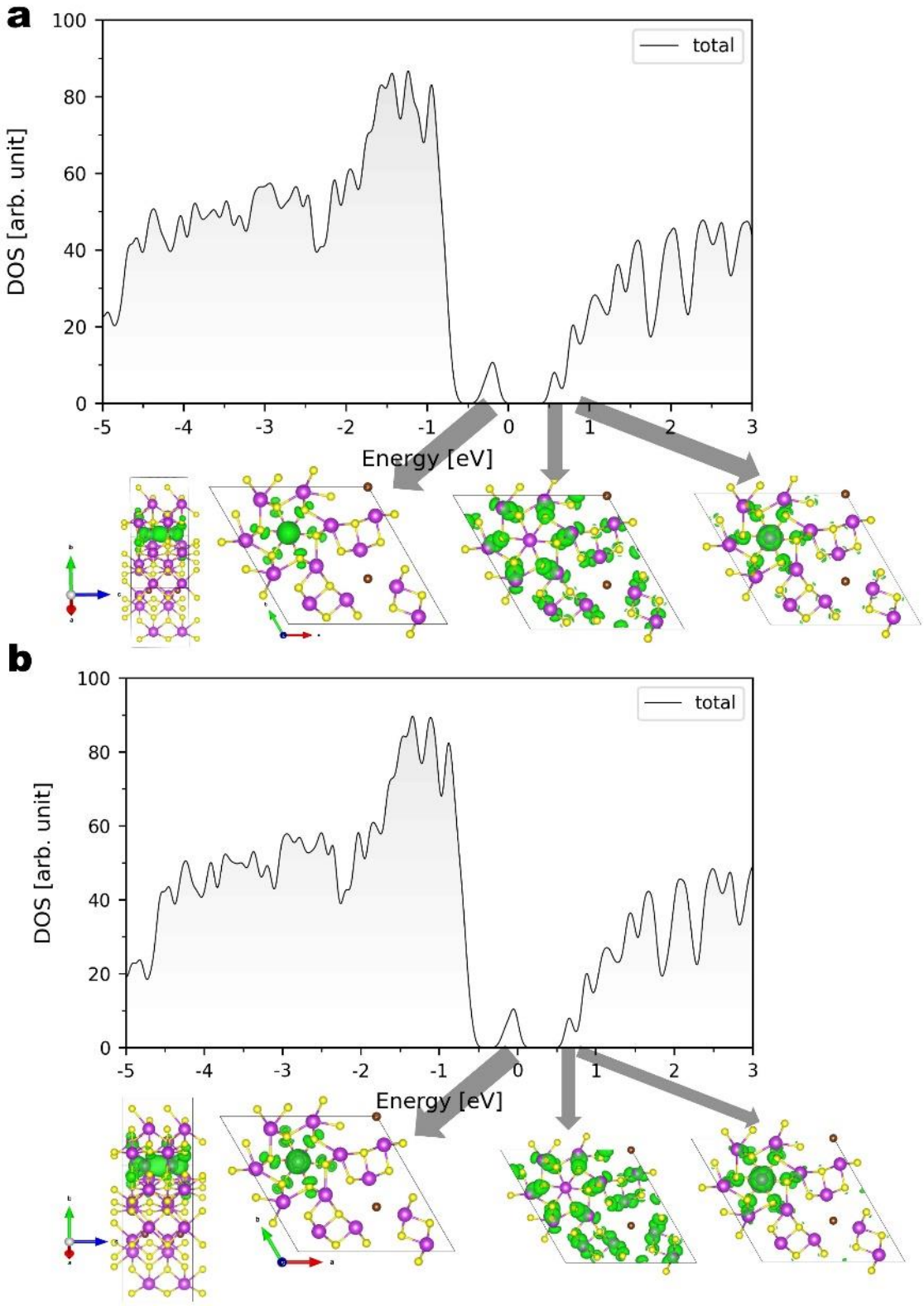

Figure S21. DOS and partial charge densities in $Bi_{13}S_{18}Br_2$ calculated including spin-orbit coupling. In panel a (b), we report the DOS and partial charge densities (green isosurfaces) calculated on the geometry obtained by neglecting (including) SOC during the optimization. The energy intervals (with respect to the Fermi level) of the partial charge densities, from left to right, are as follows. In panel a: -0.5/0.0 eV, 0.40/0.67 eV, 0.67/0.89 eV; in panel b: -0.4/0.0 eV, 0.40/0.60 eV, 0.60/0.75 eV.